Validation of Simplified Micro-models for the Static Analysis of Masonry Arches and Vaults

Validation of simplified micro-models for the static analysis of masonry arches and vaults

M. Alforno[a]*, A. Monaco[a], F. Venuti[a] and C. Calderini[b]

[a]*Department of Architecture and Design, Politecnico di Torino, Torino, Italy;*
[b]*Department of Civil, Chemical and Environmental Engineering, University of Genoa, Genova, Italy*

*e-mail: marco.alforno@polito.it

Compared to simple masonry walls, numerical modelling of masonry vaulted structures is particularly complex due to their three-dimensional curved geometry and articulated masonry pattern. Moreover, the scarce availability of experimental data make it difficult to validate numerical models for these types of structures. Recently, the simplified micro-modelling approach has been applied by different authors, despite some intrinsic limits, such as huge numerical effort and adoption of ad-hoc written numerical codes. The aim of this study is to overcome these difficulties by using a commercial software with built-in friction interface models and to validate the proposed simplified-micro model through experimental tests on in-scale specimens of arch and cross vault. The proposed approach has shown promising features: experimental results have been numerically reproduced with a high degree of accuracy, both in case of planar and space structures, with both dry and mortar joints. The final result of the study is a validated modelling strategy that could be confidently applied to real masonry vaulted structures.

Keywords: masonry; arch; cross vault; in-scale models; finite element models; simplified micro-modelling

1. Introduction

Numerical simulation of masonry structures is of crucial importance to understand the behaviour of historical constructions and, therefore, for the preservation of our architectural heritage. However, despite significant advances have been made in the last 50 years, this topic still remains an open field of research, in particular when reference

is made to complex masonry structures as arches and vaults. In fact, these structures have two additional elements of complexity compared to simple masonry walls: i) a three-dimensional curved geometry and ii) an articulated masonry pattern (Alforno et al. 2019).

For these reasons, the modelling of complex masonry arches and vaults has been traditionally tackled by means of numerical approaches according to different strategies and different levels of accuracy. A comprehensive review of the great amount of literature on computational analysis of masonry structures has been recently proposed by D'Altri et al. (2019c). Focusing the attention on masonry curved structures, the existing modelling approaches can be classified into three categories: continuum models, block-based models and geometry-based models. The latters describe the structure as a rigid body and usually adopt limit analysis-based solutions, such as the Thrust Network Analysis proposed by Block and Ochsendorf (2007). The first two categories correspond to macro-modelling and micro-modelling approaches, respectively, as defined by Lourenço et al. (1995). In macro-modelling approaches, units and mortar joints are homogenized into a homogeneous continuous material. In micro-modelling approaches, the different components of masonry are modelled separately. In particular, in detailed micro-modelling approaches blocks, mortar and mortar/block interfaces are modelled separately, while in simplified micro-modelling approach expanded units are modelled as continuum elements, while mortar joints and unit/mortar interfaces are lumped into an "average" interface.

Block-based models have recently attracted increasing attention, despite some drawbacks, which mainly consist in a huge computational demand and in the

complexity implied in the model assembly, which does not allow their use in everyday practice. Actually, this modelling approach shows some interesting features: it allows to describe in detail crack propagation and collapse mechanisms; it allows mechanical characterization of masonry constituents from small-scale experimental tests; it allows to study the effects of micro-geometrical features, such as brick pattern, on the behaviour of masonry structures, which can be important when analysing three dimensional structures like vaults (Alforno et al. 2019).

Block-based approach has recently been applied with increasing frequency, not only to small masonry assemblages, but also to larger masonry structures, such as walls and vaults. These attempts have been made not only within the framework of FEM (Milani et al. 2016, Abdulla, Cunningham and Gillie 2017, D'Altri et al. 2019), but also applying different modelling techniques, such as Distinct (or Discrete) Element Model (DEM) (Van Mele et al. 2012, McIrney and DeJong 2015, Bui et al. 2017) and rigid-block models based on limit analysis (Portioli et al. 2013, Portioli and Cascini 2017, Rossi et al. 2020, Cascini et al. 2020).

Besides numerical approaches, analytical approaches have also been developed in the field of both incremental analysis (e.g., Fabbrocino et al. 2019) and limit analysis (e.g., Riviero et al. 2013, Carr et al. 2013). The focus of this paper is on numerical approach in FEM environment.

Despite the large use of FEM commercial software in engineering practice, nowadays the study of complex masonry structures such as arches and vaults is limited to few researchers that have developed ad-hoc written codes or external subroutines linked to commercial software. This happens both in the case of macro- and micro-

modelling, where ad-hoc written constitutive laws for the homogenized material (Creazza et al. 2002, Calderini, Lagomarsino 2008, Holzer 2011, Milani and Tralli 2012) or for block-to-block interfaces (Milani et al. 2016, Smoljanovic et al. 2018, Sarhosis et al. 2018, D'Altri et al. 2019, Zhao et al. 2020) have been implemented, respectively.

The possibility to confidently use commercial software with built-in material and interface models could greatly enhance the engineers' capability to assess the structural behaviour of arched masonry structures. To this aim, reliable modelling strategies should be identified and validated. Concerning validation, one of the main difficulties lies in the scarce availability of experimental data on real scale masonry specimens (Torres et al. 2019). A valid alternative for validation is to refer to experimental tests made on in-scale specimens (Theodossopoulos at al. 2002, Theodossopoulos, Sinha and Usmani 2003, Milani et al. 2016, Rossi et al. 2017).

The aim of this study is to propose and validate a method to analyse the structural behaviour of masonry vaults by means of a simplified micro-modelling strategy, which can be easily implemented in the commercial software Abaqus (Abaqus v. 2019) using built-in interface models. The numerical method presented is aimed at simulating the static behaviour of masonry arches and vaults subjected to their self-weight and external forces/displacements, through quasi-static FEM analyses. The analysis procedure is applied to two reduced-scale benchmarks, a wood circular arch and plastic cross vault, for which experimental data were available.

The main contribution of this study lies in the validation of a modelling strategy, based on the use of a commercial software, that could therefore be adopted by a wider

audience and confidently applied to assess the structural behaviour of new or historical masonry curved structures.

The paper develops as follows: in Section 2, the adopted modelling strategy is described in detail; Section 3 is devoted to the description of the reduced-scale wood circular arch test campaign and numerical simulations; in Section 4, the reduced-scale plastic cross vault experimental campaign and numerical simulations are described and comparison with experimental results is commented on; finally, in Section 5, conclusions and research perspectives are outlined.

2. Method of analysis

The proposed method of analysis, implemented through the general-purpose FEM software Abaqus (Abaqus v. 2019), is based on three aspects: i) the accurate geometrical description of the structure, considering its actual 3D curved geometry and its block pattern; ii) the adoption of a simplified micro-modelling approach, in which the structure is schematized as a set of blocks connected by equivalent interfaces, representing the non-linear behaviour of mortar joints and real blocks/mortar interfaces; iii) the use of implicit dynamic analyses.

In the following sections, each of the three above mentioned aspects is described in detail.

2.1 Geometrical modelling

In this study, the following two types of assemblages are considered: parallelepiped blocks with wedge-shaped mortar joints (Figure 1a) and wedge-shaped dry-jointed

blocks (Figure 1d). The definition of three-dimensional blocks, according to the simplified micro-modelling approach, should be made by taking into account the actual dimensions of brick/blocks and the block pattern with which they are assembled, namely the masonry apparatus. If mortar joints are present, the geometry of the simplified block is enlarged by incorporating half the thickness of the mortar joint, as can be seen in Figure 1b, where this quite standard procedure is schematised (Lourenço et al. 1995). Conversely, if the assemblage is made of dry-jointed voussoirs, the simplified blocks coincide with the real blocks (Figure 1e). The simplified blocks are then meshed in FEM environment and interfaces are identified between blocks (Figure 1c and Figure 1f).

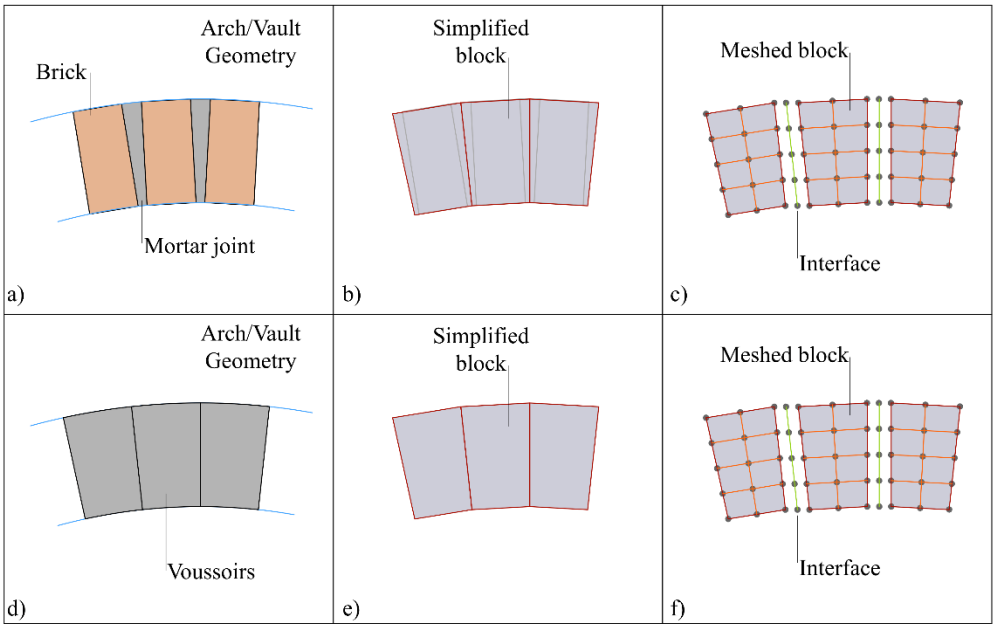

Figure 1: Geometric modelling strategies

The definition of contacts is an aspect of paramount importance in the generation of this kind of models. In particular, interactions endowed with mechanical contact properties are used for implementing the algorithms able to model contact pressures and friction that govern the relative normal and tangential motion of the surfaces.

Several approaches are available in Abaqus (Abaqus v. 2019) for defining contacts. Among them, the surface-based contact approach is used through the detection of the so-called “contact pairs”. The latter consists in the surface definitions for the bodies in contact (or that could potentially come into contact during the analysis) and the definition of the contact interaction.

In the generated model, the longitudinal and transversal faces of the blocks in contact are detected for the simulation of the interface behaviour of both bed and head joints. Among these faces, master and slave surfaces are identified to apply the contact property. Figure 2 shows an example of contact pairs for bed and head joints. In particular, the figure shows that master and slave surfaces have the same mesh and, therefore, the detection of the contacting nodes can be given with almost null tolerance error. The nodes laying on a surface have to be assumed as “master” for some contact pairs and “slave” for some others. This is due to the brick pattern in which one block (for instance block C in Figure 2) is in touch with two adjacent blocks (blocks A and B in the figure) and, therefore, the model has to take into account all combined contact pairs (i.e. contact C to A, C to B and A to B) considering both bed and head joints. In all contact definitions, the slave nodes will follow the degrees of freedom of the corresponding master nodes according to the interaction law implemented.

In the presented method, both master and slave surfaces are meshed using the same approximate element size. Since all blocks are meshed with the same element size, all six faces of the blocks have the same number of nodes (Figure 2). Moreover, a block surface that is assigned a Slave surface for one contact pair (e.g.: contact pair C-A in Figure 2), could also be assigned a Master surface for another contact pair (e.g.: contact pair C-B in Figure 2).

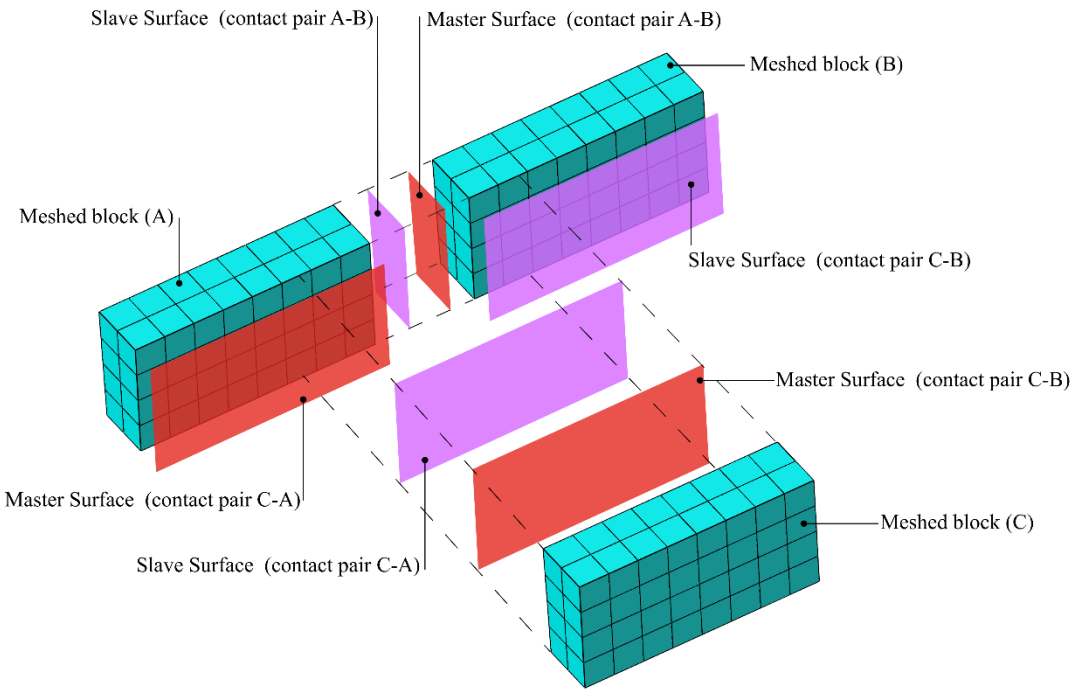

Figure 2: Master and slave surfaces for contact definition

2.2 Constitutive laws of blocks and interfaces

In the approach adopted in this study, blocks are linear elastic, while interfaces have a non-linear constitutive behaviour. The mechanical response of the interface is taken into account using built-in constitutive models available in the general-purpose FEM software Abaqus (Abaqus v. 2019). The sliding formulation adopted in the models is "finite sliding" with the surface-to-surface discretization method.

In particular, it is noteworthy to observe that, when blocks and mortar experience contact, two components should be considered, namely normal and tangential contacts. It is well known from fracture mechanics that, for quasi-brittle materials as masonry and mortar, in the interface failure mechanism normal and tangential components are generally coupled. Conversely, in this study they are assumed uncoupled for simplicity. Such assumption is supported by the observation that the collapse mechanisms of arches and vaults are mainly related to "Mode I" local failure modes, with scarce interaction

with “Mode II” failure modes. This has been largely demonstrated not only for arches, but even for masonry vaults subjected to shear actions (Rossi et al. 2016, Milani et al. 2016). Conversely, a different modelling procedure should be adopted for other applications such as the modelling of masonry panels under in-plane and out-of-plane loading, in which the collapse is highly influenced by the coupling of the interface constitutive law in normal and tangential direction (Abdulla et al. 2017, D’Altri et al. 2018, D’Altri et al. 2019).

In the presented model, the tensile strength is null, while the normal contact in compression is described through a linear elastic behaviour with high (almost infinite) normal stiffness, and the tangential behaviour is implemented through a purely frictional model. Both approaches are herein described in detail.

The normal contact in compression is assumed rigid, both in case of dry joints and mortar joints. In the latter case, the deformability of the mortar layer is accounted for through the elastic modulus of the expanded block. The almost rigid normal contact is modelled through the implementation of a penalty method, in which quite high values of normal stiffness k_n are used after proper calibration.

The penalty method used in the normal compression can be read as:

$$\sigma_c = k_n \bullet \delta_n \tag{1}$$

where σ_c is the normal compressive stress and δ_n is the corresponding normal displacement. The implementation of a penalty method for the normal contact implies that a small level of mutual penetration between nodes into contact can occur. However, even in the absence of specific procedures aimed at avoiding this phenomenon, if sufficiently high normal stiffness values are adopted, the penetration between nodes is negligible. Conversely, the implementation of the penalty method in normal

compression results in a very efficient tool for improving the convergence of the performed analyses.

When normal and tangential relative displacements occur, contact can be defined through the combination of cohesive and frictional behaviour. This approach has been adopted by several authors such as Milani et al. (2016), Abdulla et al. (2017) and D'Altri et al. (2018, 2019a, 2019b), who employed subroutines or user defined codes to develop the interface material model as combination of the two effects. However, when the influence of the cohesion is limited (for instance, dry joints or joints made by low-cohesive mortar), the interaction between cohesive and frictional response is not significant and the global response is mainly dominated by friction. Therefore, in the present study the tangential interface behaviour is modelled using the friction model only, to relate the maximum allowable frictional shear stress to the contact pressure, according to the following law:

$$\tau_{fr} = -\sigma_c \bullet \mu \tag{2}$$

where τ_{fr} represents the frictional shear stress and μ is the coefficient of dry friction. According to its basic formulation, the friction model defines the limit between sticking and sliding state of contacting surfaces assuming isotropic friction, i.e. adopting the same value of static friction coefficient in all directions. The stick-slip numerical calculations determine when a point transitions from sticking to slipping or vice versa. In the case of three-dimensional simulations, two components of shear stress have to be considered, τ_1 and τ_2, each one acting in the corresponding local tangential direction. In such cases, an equivalent shear stress is defined as $\tau_{eq} = \sqrt{\tau_1^2 + \tau_2^2}$ and used for the

stick-slip calculation. Consequently, a surface can be defined in the contact pressure-shear stress space, along which a point transitions from sticking to slipping.

The choice of neglecting the tensile strength and cohesion of masonry joints is quite common in historical masonry constructions, in particular when masonry arches and vaults with dry or low-strength lime mortar joints are considered. Except for particularly slender and light curved masonry elements, where the tensile strength cannot be neglected (Ramaglia et al. 2016), many studies have demonstrated the limited influence of this parameter in the failure mode and crack pattern of masonry vaulted structures. Recent studies in the literature had also shown the limited effect of the cohesion in vaults subjected to shear tests (D'Altri et al. 2019).

In conclusion, considering the two components (blocks and interfaces) of the proposed modelling strategy, the following parameters should be defined:

- Young modulus (E), Poisson coefficient (v) and material density (ρ) of the blocks;
- normal stiffness of the interfaces (k_n);
- friction coefficient of the interfaces (μ).

In general, due to the difficulties in assigning a reliable value to the normal stiffness of the interfaces k_n and considering that penalty method for normal contact requires the adoption of high normal stiffness values, in the proposed strategy the normal stiffness of the interfaces should be calibrated in order to have an almost rigid response compared to that of the blocks. Thus, given the Young modulus of the blocks, k_n can be obtained by performing convergence analysis, i.e. evaluating the structural

behaviour for increasing value of k_n until convergence on a response parameter (e.g. displacement at one abutment) is obtained.

The adoption of almost rigid interfaces in compression implies to concentrate in blocks the entire elastic deformability of the system. For this reason, the Young modulus *E,* as well as the Poisson coefficient and material density, assigned to blocks should not be defined considering one block only, but considering the actual masonry composite made of blocks, masonry joints (if present) and interfaces. In this way, both dry and (low strength) mortar joints masonries can be modelled with the same approach.

In the framework of micro-modelling approaches, the proposed strategy presents different advantages. On the one hand, it is based on few and clear parameters (E, v, ρ and μ), that can be easily estimated by experimental tests on small assemblages. On the other hand, it avoids the problem of experimentally defining the interface deformability (k_n) related to both dry and mortar joints. Moreover, the proposed approach limits the issues related to scale-effects only to few parameters, i.e., the elastic modulus and material density of the masonry assemblage. Finally, it allows quite fast and stable numerical analyses to be performed.

2.3 Type of analysis

In the presented method, the analysis is performed in two different steps: firstly, the structure is subjected only to its self-weight, subsequently external forces or imposed settlements are applied. The second analysis step assumes as initial conditions for the analysis the configuration of the structure, as it results from the last increment of the first analysis step.

In order to solve the convergence issues that typically arise in contact problems, the numerical calculation procedure adopted is the dynamic implicit analysis, which uses implicit time integration to calculate the transient dynamic response of a system. In the present case, the load application is performed in quasi-static manner, forcing the introduction of inertia effects primarily intended to control and normalize unstable behaviour in analyses mainly focused on the static structural response. The structural problem analysed in this research can be indeed considered "inertial" because the response time sought is long compared to the time required for waves to traverse the structure, in contrast to some other engineering problems such as wave propagation solutions associated with relatively local response in continuum solids. Therefore, while in explicit schemes the stability limit of the solution is approximately equal to the time required to an elastic wave to cross the smallest element dimension in the model, in the implicit method the time step size required to obtain a stable equilibrium condition at every increment is typically one or two orders of magnitude higher. Numerically, the possibility of removing this upper bound on time step size is reached by solving nonlinear equations, whose accuracy however reduces for increasing time step size.

In the present model, the time step for the implicit integration is chosen automatically using the concept of "half-increment residual" (Hibbitt and Karlsson, 1979), which basically allows monitoring the values of equilibrium residuals at the time $t + \Delta t/2$ once the solution at $t + \Delta t$ has been obtained: so doing, the accuracy of the solution can be evaluated and the time step size can be properly adjusted by consequence.

The equilibrium equation solver used in the model makes use of an asymmetric matrix storage and adopts the Full Newton solution technique. Parallelization on

multiple processors is also performed, depending on the computational performance available on the machine used to run each analysis.

By default, the load variation with the analysis time is assumed to be linear, meaning that the process is essentially monotonic: the solver uses a linear extrapolation in time of the previous incremental solution to begin the nonlinear equation solution of the following increment.

Finally, in case of large displacement analyses the geometrical nonlinearities are considered.

3. Reduced-scale wood circular arch

3.1. Description of the model and experimental test

The first case study is a 1:6 scale model of a circular arch, which has been built at the Politecnico di Torino (Figure 3). The arch span length is 0.62 m and the rise-to-span ratio is 0.3. The arch geometry coincides with the one of the head arches in the 1:5 scale model of masonry cross vault described in Rossi et al. 2016 and analysed in the following section. The arch blocks of dimensions 0.5x1x2 cm are made of wood and are varnished with waterproofing paint, in line with the experiments described in Theodossopoulos et al. 2002 and D'Altri et al. 2019. They represent in scale the typical dimensions of brick blocks (6x12x24 cm). The wooden blocks are bonded by mortar, made of three parts of sand, one part of lime and one part of water, as in D'Altri et al. 2019. Bricks are laid so that the arch thickness is 1 cm.

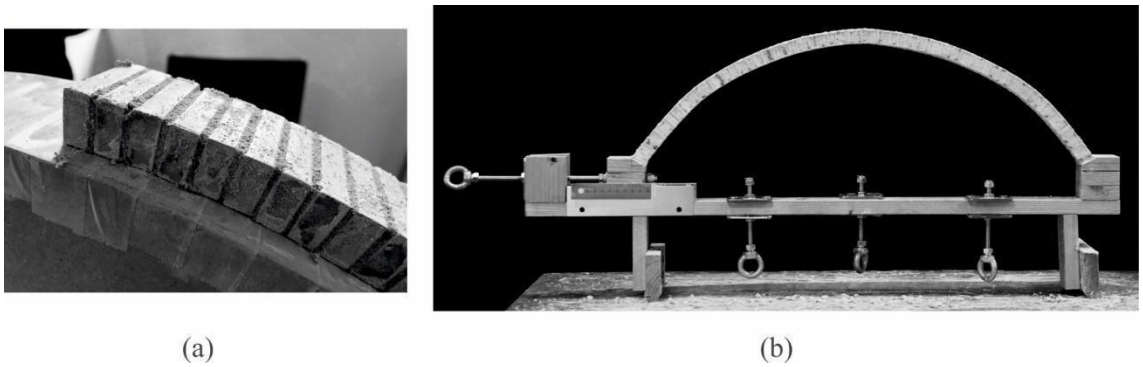

Figure 3: the arch during construction (a) and after removal of scaffolding (b)

The testing device was designed to perform opening tests (Figure 3b): one abutment is fixed, while the other can be moved horizontally by simply turning a ribbed bar. The scaffolding can be mounted on the frame that links the two abutments and easily removed after completion.

The test has been video recorded and pictures have been taken at each step of imposed displacement (every 2 mm). The abutment displacement has been recorded with a digital calliper. The ultimate displacement of the moving abutment is 13.74 mm, corresponding to a displacement to span ratio equal to 2.22%. It is worth noting that the theoretical collapse mechanism should involve the symmetrical formation of five hinges. In the experimental campaign, the collapse mechanism involves only four hinges, as can be seen in Figure 4: the experimental asymmetrical collapse mechanism could be due to geometrical imperfections, as already observed by other authors (Ochsendorf 2002).

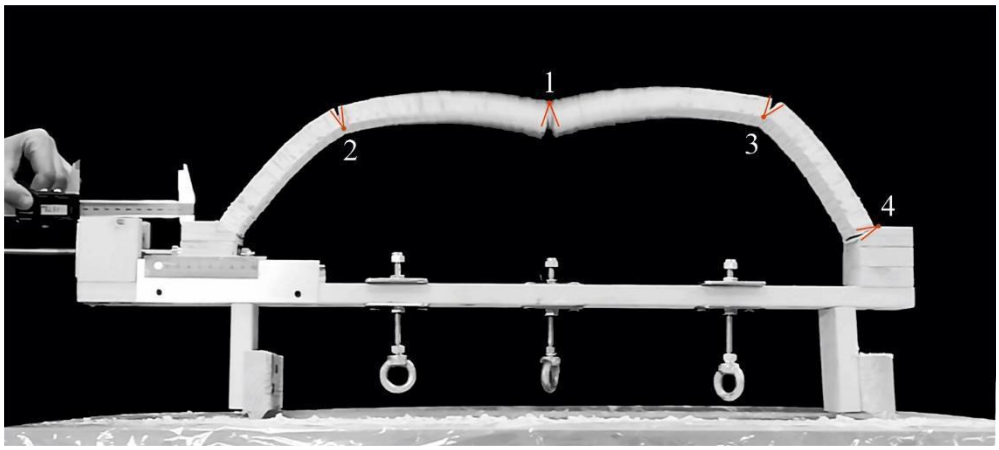

Figure 4: formation of 4 hinges before collapse

3.2. Numerical modelling

The mechanical model of the circular arch is built according to the simplified micro-modelling approach described in Section 2. It is worth noting that, under the hypotheses of i) no tensile strength and no cohesion of interfaces, ii) infinite compressive strength of blocks and iii) almost rigid blocks and interfaces, the behaviour of masonry structures relies only on their geometry and scale-effects can be neglected. For this reason, if blocks are stiff enough, the proposed modelling strategy may be considered as scale-independent and thus easily applied to reduced-scale models. In this case, expanded blocks that account for the 2 mm thickness of the mortar joints have been considered. The finite elements used for the blocks are linear hexahedra of 6 mm size; both abutments are pinned and a horizontal displacement is applied to one of them, constraining all other degrees of freedom. Numerical analysis is performed in two steps: in the first one, dead load is applied; in the second one, horizontal displacement u_x at one of the abutments is progressively imposed to simulate the experimental set-up.

The mechanical properties of the blocks and of friction interfaces between blocks are summarised in Table 1. Since no experimental tests were specifically

performed to determine the mechanical properties of the adopted blocks and interfaces, all the reported values, except k_n, have been taken from Carfagnini et al. 2018 and D'Altri et al. 2019, where experimental tests with assemblages of similar wood blocks and mortar were performed.

Table 1: mechanical properties of blocks and interfaces for the wood arch

Blocks			Interfaces	
ρ [kg/m^3]	E [MPa]	v [-]	μ [-]	k_n [N/m^3]
700	570	0.2	0.5	$5 \cdot 10^{12}$

The value of the normal stiffness k_n was calibrated through a convergence analysis, where the displacement at collapse u_c has been determined for different values of k_n in the range $5 \cdot 10^9$-$5 \cdot 10^{15}$ N/m^3. Figure 5 plots u_c versus k_n: the ultimate displacement remains almost constant for values of k_n above $5 \cdot 10^{12}$ N/m^3. Therefore, this value is the one corresponding to almost rigid contact, and thus it has been employed for the following analyses.

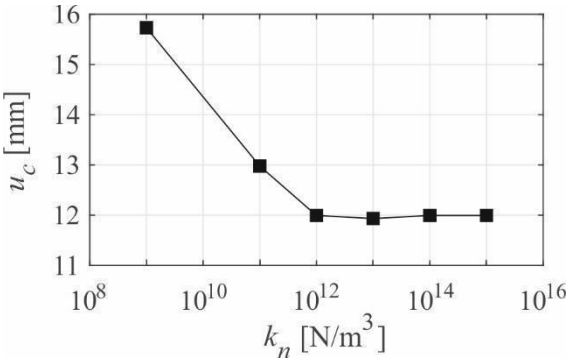

Figure 5: displacement at collapse versus k_n

Figure 6 compares the collapse mechanism in experimental test and numerical simulation. The collapse mechanism observed in the numerical model consists in the simultaneous opening of two hinges at the abutments, resulting in a five-hinge collapse mechanism (Figure 6). In Figure 7, the force-displacement curve of the numerical arch is represented. It can be observed that the collapse cannot be easily defined on the curve. The drops and jumps of the load-displacement curve are due to the formation of hinges in the arch and their progressive translation from one joint to another, according to the expected collapse mechanism (see also Figure 9). The energy release due to the formation of such hinges induces some numerical instabilities which locally affects the global load-displacement curve. For this reason, the collapse has been visually identified in correspondence of the simultaneous opening of the hinges number 4 and 5 (Figure 7, red circle). The numerical imposed displacement at collapse u_c equals 12.82 mm, which is 6.7% lower than the one registered experimentally (13.74 mm).

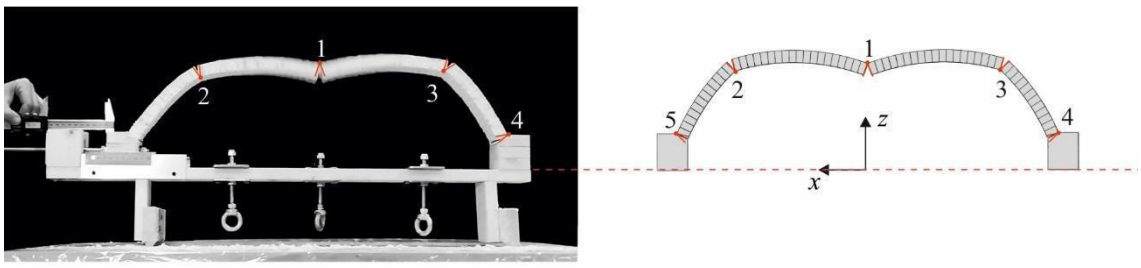

(a) (b)

Figure 6: comparison between collapse mechanism in experimental test (a) and numerical simulation (b)

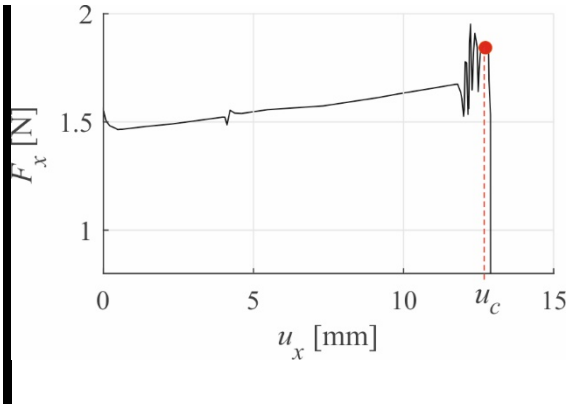

Figure 7: numerical load-displacement curve

Figure 8 compares the deformed shapes in experimental test and numerical simulation for an imposed displacement of about 12.10 mm, corresponding to the last recorded picture before collapse. The numerical deformed shape agrees quite well with the experimental one, both in terms of vertical displacement at the key and in terms of position of hinges number 1, 2 and 3. It is worth noting that, in the experimental test, the hinge number 2 is not symmetrical with respect to the hinge number 3 and opens nearer to the moving abutment. This asymmetry is reasonably due to geometrical imperfections, as already pointed out in Section 3.1. Actually, the position of hinges number 2 and 3 changes during the evolution of the collapse mechanism also in the numerical simulation, as shown in Figure 9. In particular, they progressively move towards the key.

In conclusion, the adopted micro-modelling approach has proved to be quite reliable in simulating a simple bi-dimensional collapse mechanism. Note that, in the opening mechanism of the arch, the friction behaviour of interfaces is expected to play a minor role. Therefore, the complete validation of the proposed interface model should be done considering different loading conditions and more complex structure. This will be done in the next section.

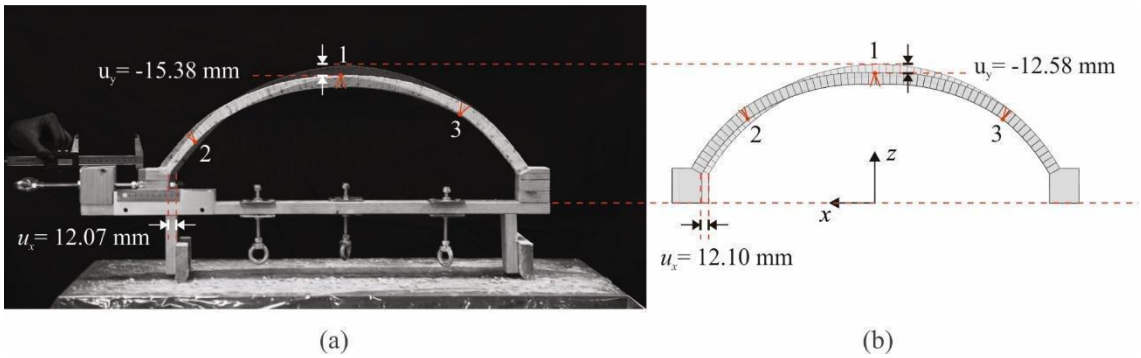

Figure 8: comparison between deformed and undeformed arch in experimental test (a) and numerical simulation (b)

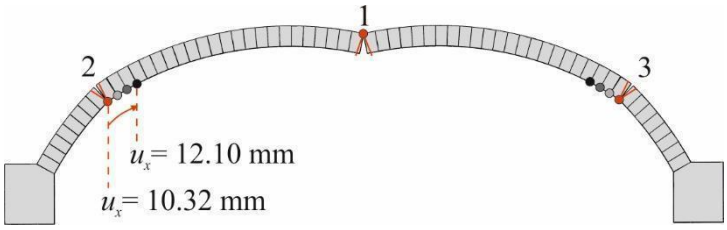

Figure 9: evolution of the collapse mechanism in numerical simulation for imposed displacement from 10.32 to 12.10 mm.

4. Reduced-scale plastic cross vault

4.1. Description of the model and experimental tests

The second case study is the 1:5 scale model of a cross vault built at the University of Genova and described in Rossi, Calderini and Lagomarsino 2016 and Milani et al. 2016 (Figure 10). The cross vault has a square base, generated by the intersection of two semi-circular barrel vaults. The net span is approximately 0.62 m, the rise is about 0.225 m and the vault is made of typical brick blocks (6 x 12 x 24 cm, on a scale of 1:5). The model is assembled with dry joints; therefore, the blocks have been designed in stereotomy. The plastic blocks are made by a 3D prototyping technique called Selecting

Laser Sintering. Inside each block a steel plate was inserted in order to increase the vault self-weight to provide stability under accidental actions.

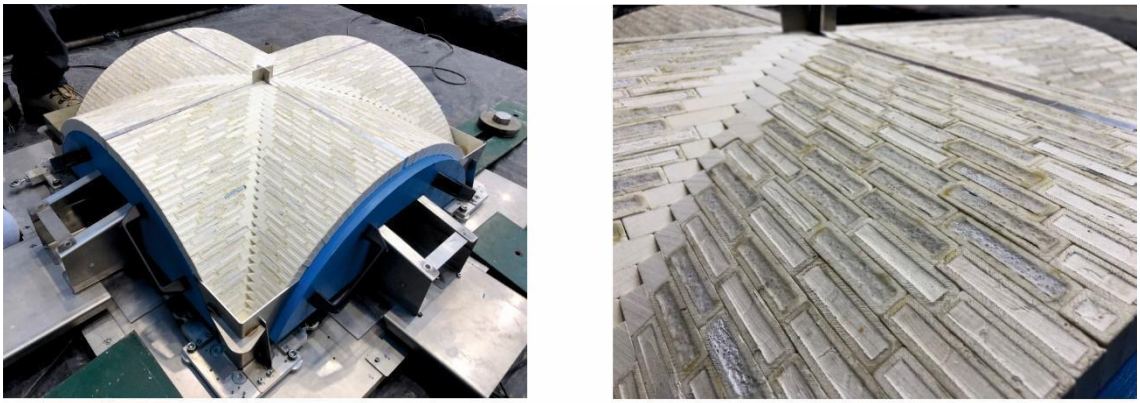

(a) (b)

Figure 10: the cross vault before scaffolding removal (a) and detail of the blocks (b)

The model was used to perform several tests, aimed at simulating the typical collapse mechanism of vaults due to static settlements of the abutments or to seismic action. For the aim of the present study, the following will be considered (the interested reader can refer to the original papers for more details): the longitudinal opening test (OT), the simple shear test (ST) and the tilting-plane test (TT). The adopted experimental set-ups are schematised in Figure 11 and Figure 12.

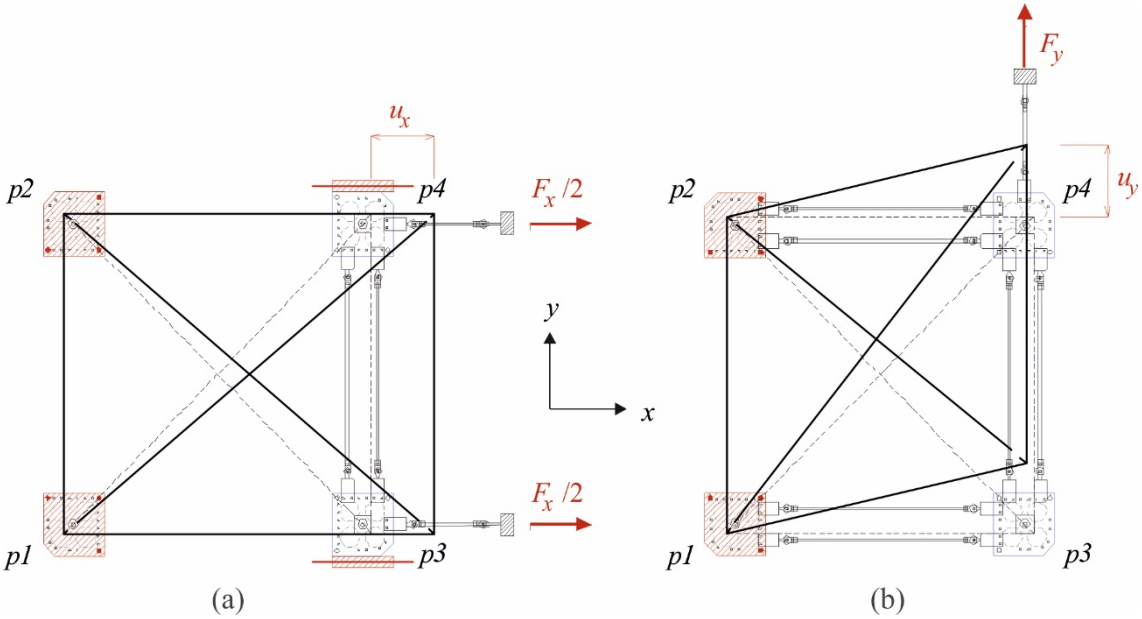

Figure 11: experimental set up of OT (a) and ST (b)

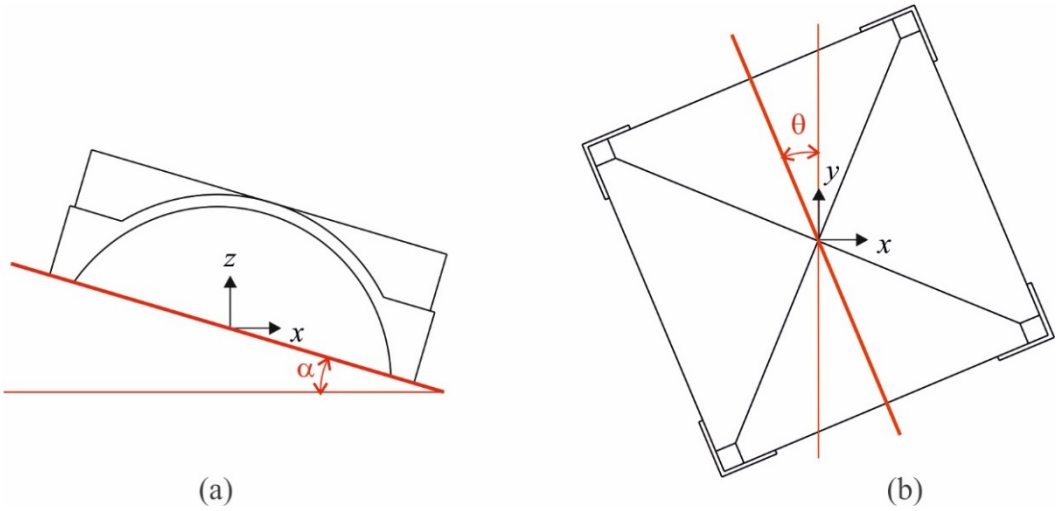

Figure 12: experimental set up of TT in lateral (a) and plan (b) views

The testing device consisted of a special frame composed of four steel squared plates, where the abutments of the vault were rigidly constrained. The testing device allowed to measure both the imposed displacement and the horizontal forces at the abutments. In the OT and ST two abutments are fixed, while the other two are moved

along the x and y axis, respectively. In the ST, the four plates are linked to each other by means of aluminium bar couples acting as tie-rods.

In the TT (Milani et al. 2016), performed to simulate seismic direct action, the four abutments are fixed and the plane where the vault lies is progressively inclined of an angle α (Figure 12a), thus producing horizontal forces proportional to the masses. In order to simulate different directions of the seismic action, the test was performed in different configurations, by varying the angle θ between the axis of rotation of the tilting plane and the axes of symmetry of the vault (Figure 12b).

4.2. Numerical modelling

The geometrical model of the cross vault has been generated with Rhinoceros. The block size and dimensions are the same as in the plastic model, except for the blocks along the diagonal arches (Figure 13a), which were modified in order to simplify the subsequent definition of interfaces. Moreover, during construction of the plastic model in laboratory, some geometrical adjustments had to be made, and ad-hoc-shaped blocks were added in the middle of the four webs (see darker blocks in Figure 10a). These modifications of the initial geometry were not accounted for in the numerical simulation. The geometrical model has been imported in Abaqus (Abaqus v 2019) for the generation of the mechanical model (Figure 13b). The finite elements used for the bricks are linear hexahedra of 6 mm size, while the blocks along the diagonal arches and in the abutments are modelled using second order tetrahedra of the same approximate size. For the hexahedral elements the meshing technique is of structured type, while for the tetrahedra a free meshing algorithm has been adopted. The model used for ST is provided of additional elements to simulate the aluminium rods that link

the four abutments. Each rod is modelled as a 1D truss element with circular section of area 1.49e-2 mm^2 and the following mechanical properties: material density ρ = 2700 kg/m^3, elastic modulus E = 64000 MPa and Poisson coefficient ν = 0.3. Each abutment lies on an aluminium plate, which is rigidly constrained at the base and to which the aluminium rods are pinned. In order to simulate the constraint given by the angular aluminium plates, which have been inserted in the physical model in order to confine the first seven courses of bricks (Figure 10a), rigid tie elements connect the blocks of the first seven courses to the abutments.

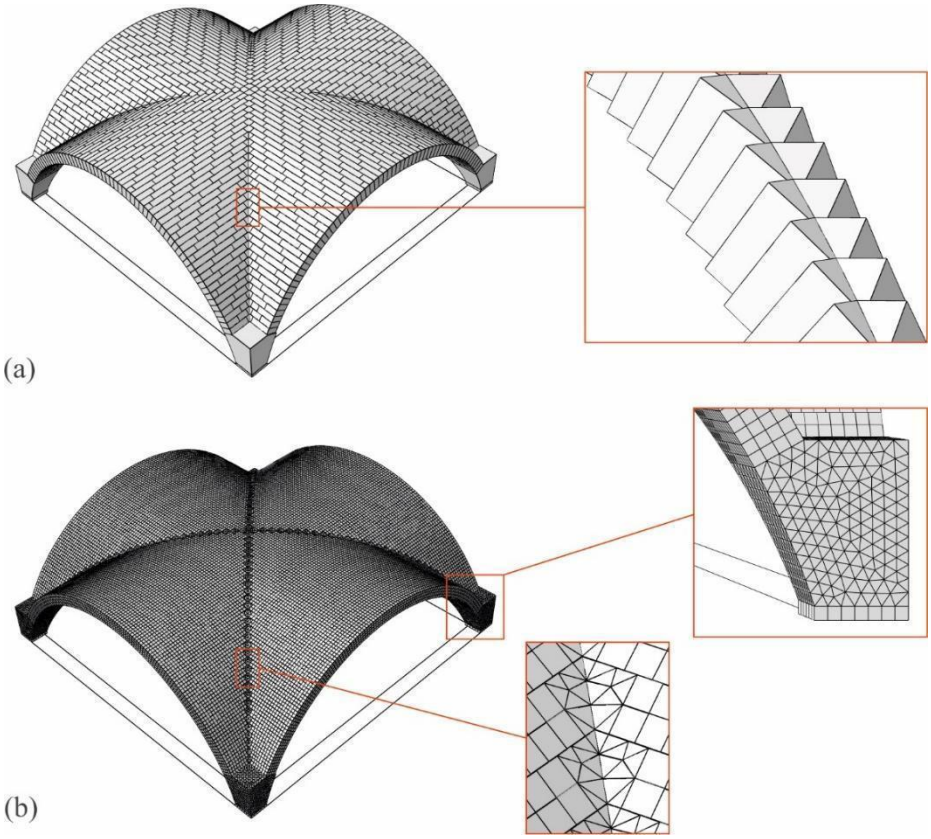

Figure 13: geometrical (a) and finite element model (b) of the cross vault

The mechanical properties of bricks and interfaces reported in Rossi, Calderini and Lagomarsino 2016 are summarised in Table 2 and highlighted in bold. The elastic

modulus E was obtained by compression tests on masonry pillars made of six blocks. This means that it is an overall elastic modulus, taking into account the deformability of both plastic blocks and interfaces. The load-displacement curves from three compression tests are reported in Figure 14. The elastic modulus of 120 MPa reported in Rossi, Calderini and Lagomarsino 2016 was estimated as the slope of the curve steeper branch, averaged on the three curves (E_4 in Figure 14b). The non-linear trend of the load-displacement curves suggest a possible overestimation of this value. Therefore, in the following subsection, a parametric analysis is performed by considering three other values of the elastic modulus (Table 2, Figure 14b): E_1 = 20 MPa, which is the tangent stiffness at the origin; E_2 = 40 MPa, being the secant stiffness corresponding to a compression of 1 kN; E_3 = 80 MPa, which is the secant stiffness corresponding to the apex of the load-displacement curve. These values have been calculated for each curve and then averaged.

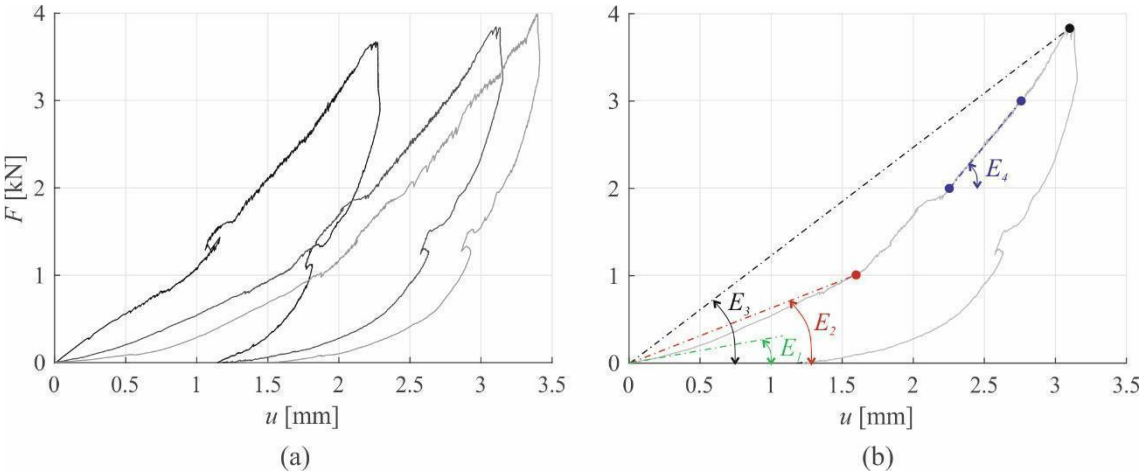

Figure 14: load-displacement curves from compression tests on six-block assemblages (a) and adopted criteria for calculation of the elastic modulus (b)

Concerning the contact stiffness k_n, its value, as already stated, should be calibrated in order to simulate an almost rigid contact. To do so, a convergence analysis has been carried out for each of the two extreme values of E (i.e. 20 and 120 MPa). Due to the high computational effort that this analysis would require if performed on the entire vault model, a circular arch that coincides with the vault's head arch was used instead. Similarly to the previous convergence analysis carried out on the wood circular arch, the analysis consists in an imposed horizontal displacement of one support. The displacement at collapse u_c has been determined for increasing value of k_n in the range $5 \cdot 10^8$-$5 \cdot 10^{15}$ N/m^3. Figure 15 plots, for each value of E, the displacement at collapse u_c versus k_n and the load-displacements curves obtained for $k_n = 5 \cdot 10^{10}$ N/m^3. The ultimate displacement remains almost constant for values of k_n above $5 \cdot 10^{10}$ N/m^3 for both considered elastic moduli. Therefore, this latter can be considered as the minimum value to have almost rigid contacts.

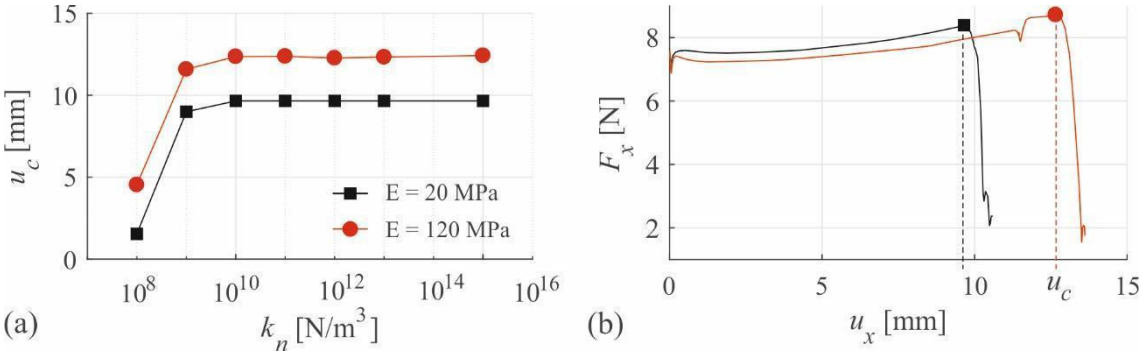

Figure 15: displacement at collapse versus k_n (a) and load-displacement curves for $k_n = 5 \cdot 10^{10}$ N/m^3 (b)

However, it can be noted from Figure 15a that there is a negligible difference in the estimation of the ultimate displacement for $k_n = 5 \cdot 10^9$ N/m^3 and $k_n = 5 \cdot 10^{10}$ N/m^3. From trial analyses it has been assessed that this difference is negligible also for the

vault, but the use of $k_n = 5 \cdot 10^9$ N/m^3 instead of $k_n = 5 \cdot 10^{10}$ N/m^3 dramatically reduces the computational effort of the analyses. Specifically, the estimated user times correspond to $1.11 \cdot 10^5$ s (30.8 hrs) and $2.85 \cdot 10^5$ s (79,1 hrs), respectively, which means a computational effort 2.5 times higher in the second case. For this reason, the value $k_n = 5 \cdot 10^9$ N/m^3 has been used in all the subsequent analyses.

Blocks			Interfaces	
ρ [kg/m^3]	E [MPa]	ν [-]	μ [-]	k_n [N/m^3]
2700	20-40-80-**120**	**0.2**	**0.56**	$5 \cdot 10^9$

Table 2: mechanical properties of blocks and interfaces for the plastic vault

In the following subsections, numerical simulations of the three experimental tests described in Section 3.2 are shown. In all cases, the analysis is performed in two steps, the first being the dead load condition. Regarding this condition, Figure 16 plots the vertical displacements due to dead load with E = 80 MPa. For this set up, the maximum vertical displacement at the key is about 3.6 mm. This value is much smaller than the one observed experimentally, as it will be discussed in the next paragraph.

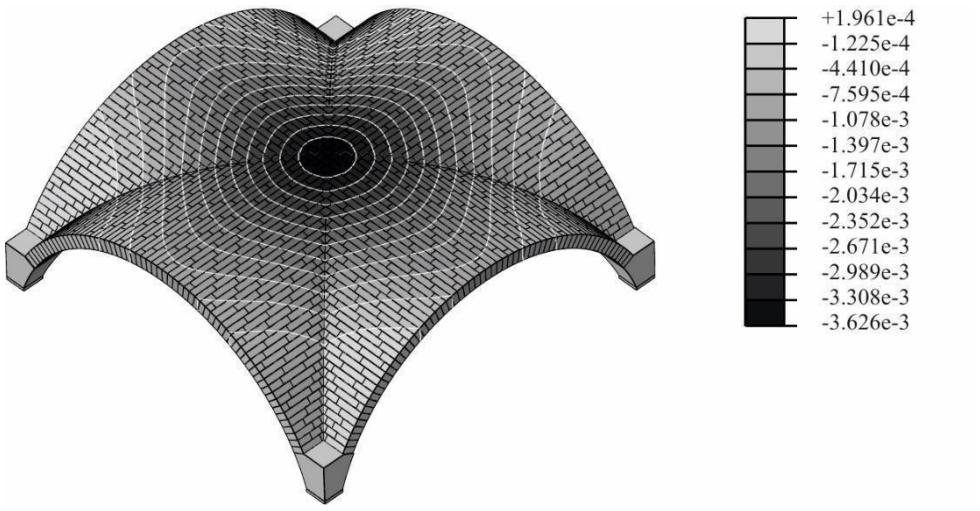

Figure 16: contour plot of vertical displacements [m] due to dead load

4.2.1. Opening test (OT)

In the numerical simulation of the OT, two abutments are fixed, while the other two are subjected to an imposed displacement u_x. A parametric analysis was carried out, by varying E in the range 20-120 MPa (Figure 17). In all cases the qualitative trend of the numerical curves well fit the experimental ones. Even though the curve obtained for the highest values of E provides the best approximation to the experimental curves in terms of resistance, it highly overestimates the ultimate displacement, which is about 70% higher than the experimental one. A possible reason for this discrepancy could be found in the overestimation of the block elastic modulus. Figure 17 shows that decreasing values of E correspond to an increase in resistance and a decrease in the ultimate displacement.

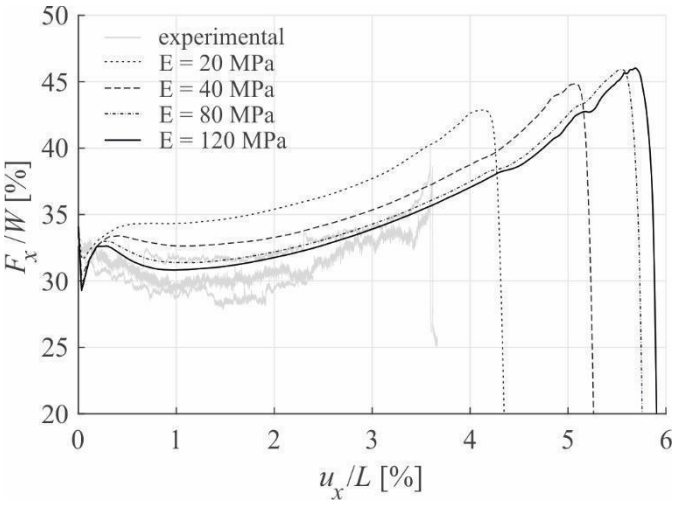

Figure 17: load-displacement curves for different values of E

A deeper insight into the obtained results is provided by looking at the deformed shapes, which are plotted for the case with E=80 MPa. Figure 18 shows the evolution of the collapse mechanism starting from the opening of the first hinge at the key. Figure 19

compares the numerical and experimental collapse shapes, together with the undeformed geometrical configuration (in light). The numerical one corresponds to an imposed displacement u_x = 35 mm, when the three-hinge mechanism highlighted in Figure 19 begins. The numerical and experimental collapse shapes show a surprising similarity. Moreover, what clearly emerges by comparing Figure 19a and Figure 17b is that the initial geometry of the plastic model displays a deviation from the ideal geometry due to a lowering of the crown (blue arrows in Figure 19a). The latter is due to the vault settlement due to dead load after scaffolding removal, and seems to be quite higher than the vertical displacement at the crown estimated numerically (Figure 16). This geometrical imperfection, probably due to the new blocks added during construction, could be a further reason for the discrepancy between experimental and numerical ultimate displacement.

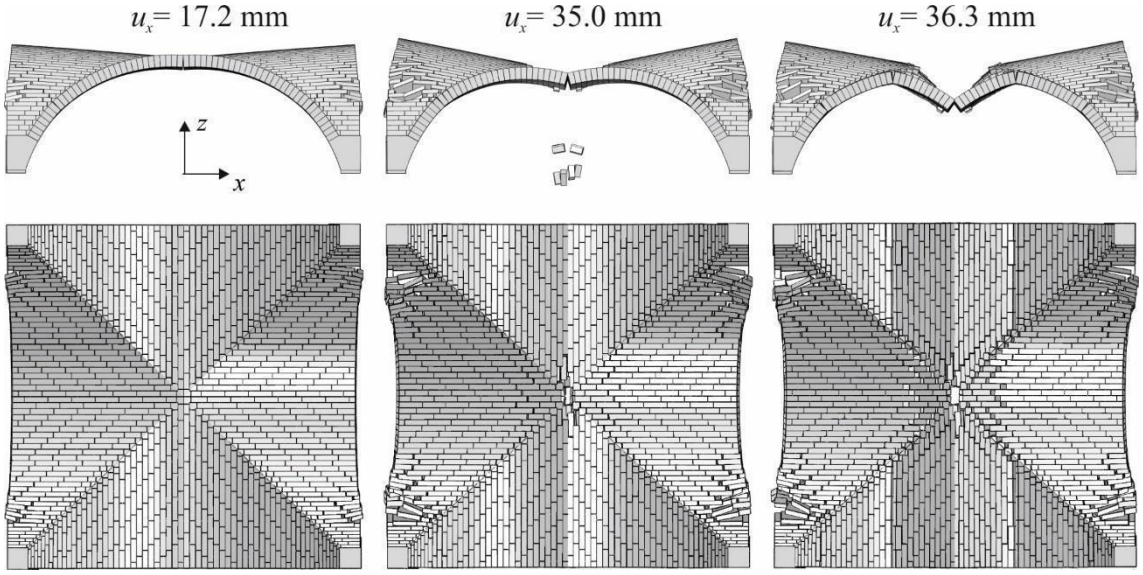

Figure 18: evolution of the collapse mechanism in numerical simulations

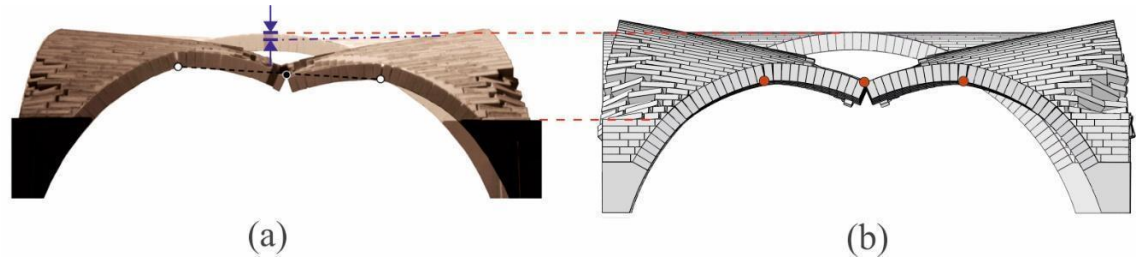

Figure 19: comparison between collapse shapes in experimental test (Rossi, Calderini and Lagomarsino 2016) (a) and numerical model (b)

4.2.2.Shear test (ST)

In the numerical simulation of the ST, a parametric analysis on the elastic modulus *E* has been performed as in the OT. The obtained results in terms of load-displacement curves are plotted in Figure 20. A very good agreement between numerical and experimental results can be observed. In this case, a decrease in the elastic modulus corresponds to a decrease in the vault resistance, while the ultimate displacement slightly changes and well fits the experimental one, whichever the value of *E*. The value of *E* that corresponds to the best fit to the experimental data is 80 MPa. This value will, therefore, be retained in the following analyses.

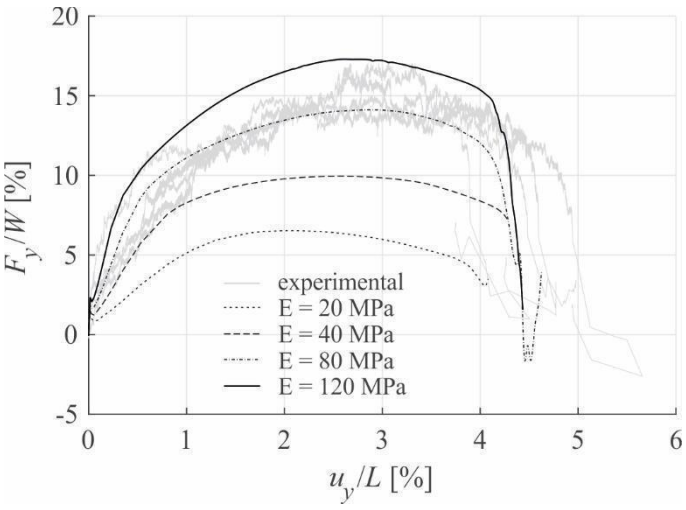

Figure 20: load-displacement curves for different values of *E*

The agreement with experimental results is also evident by looking at the collapse shapes. In Figure 21, the collapse mechanism is plotted in side and plan view (note that the numerical deformed shape is specular with respect to the experimental one). The numerical model is able to perfectly predict the position of the hinges in the perimetral arch and the crack formation along the diagonal arches.

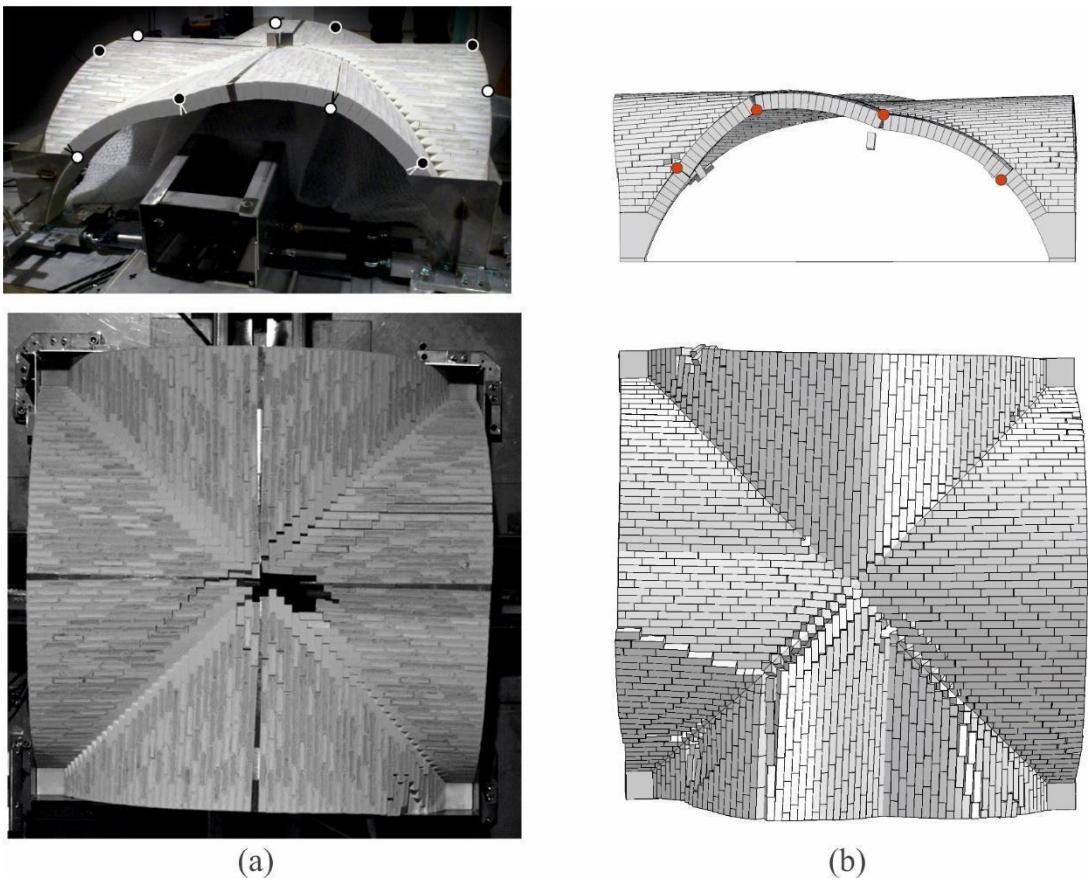

Figure 21: comparison between collapse shapes in experimental test (Rossi, Calderini and Lagomarsino 2016) (a) and numerical model (b)

4.2.3. Tilting-plane test (TT)

Finally, the TT is numerically simulated for three different values of the azimuthal angle θ [0, 22.5, 45]°. The mechanical properties of blocks and interfaces are those selected

from previous analysis, i.e., E=80 MPa and $k_n = 5 \cdot 10^9$ N/m^3. In the experimental set-up, the progressive inclination α of the horizontal plan where the vault is rigidly fixed has the effect of inducing a progressive decrease of the vertical component of the gravity acceleration and, in turn, an increase in the horizontal component. Specifically, the vertical component of g decreases proportionally to cosα, while the horizontal one increases proportionally to sinα (Figure 22).

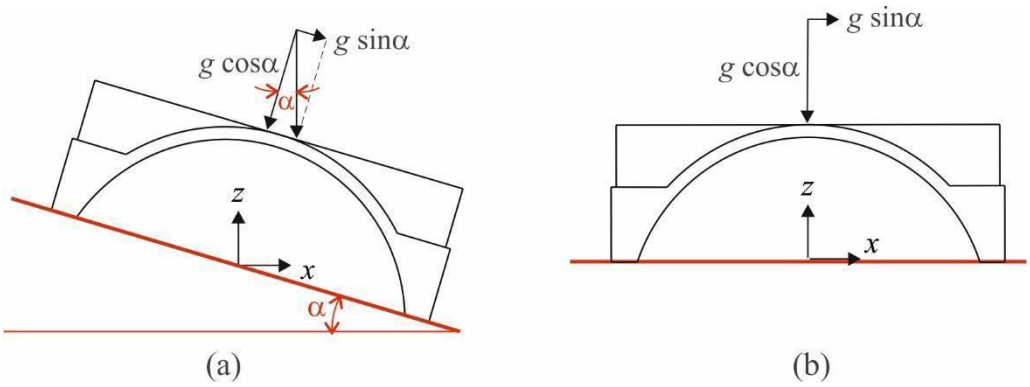

Figure 22: scheme of the TT gravity load in the experimental (a) and numerical (b) set-ups

Figure 23a plots the resultant of the reaction forces at the abutments in the xy plane versus α for each θ direction while Figure 24 shows the corresponding collapse shapes. The collapse angle α_c is estimated as the one corresponding to the peak value of F_{xy}. The obtained values of α_c are plotted in Figure 23b versus θ. Similarly to the OT, the numerical ultimate capacity overestimates the experimental one, probably due to geometrical imperfections. Nevertheless, the collapse mechanism almost perfectly reproduces the experimental one, as shown in Figure 25.

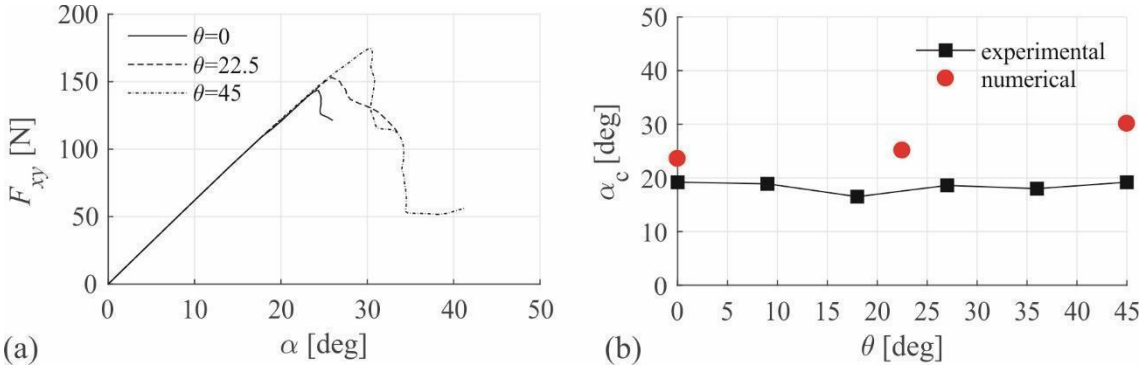

Figure 23: load-rotation curves (a) and collapse angle α_c versus θ (b)

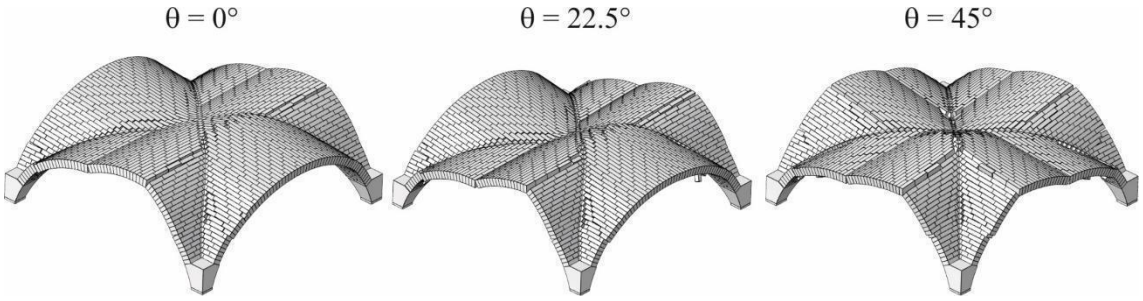

Figure 24: collapse mechanism in TT for different value of θ

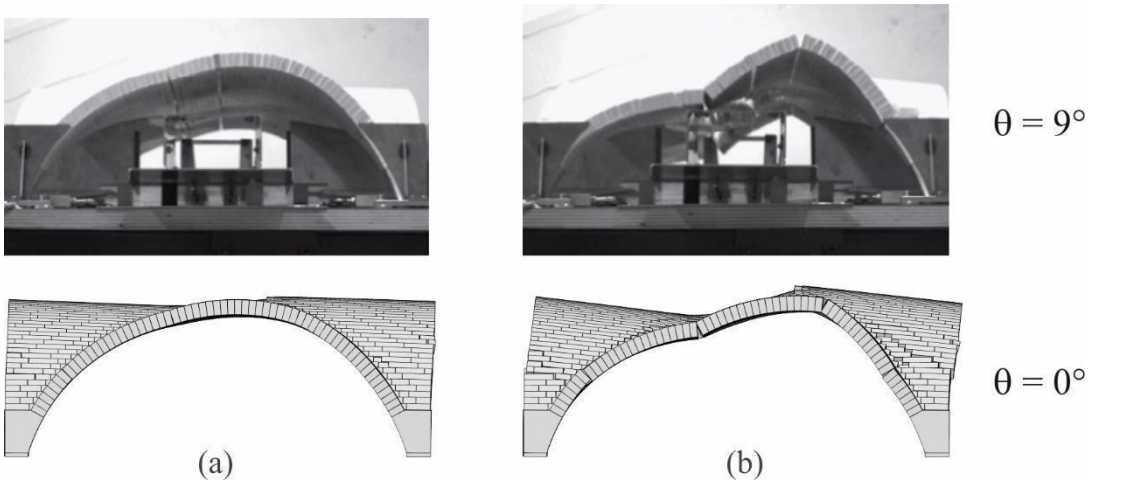

Figure 25: comparison between collapse shapes in experimental test (Milani et al. 2016) and numerical model at the step of incipient collapse (a) and during collapse (b)

5. Conclusions

This paper has proposed a simplified micro-modelling approach applied to numerical simulation of masonry arches and vaults. The approach has been implemented through the commercial software Abaqus, by adopting a built-in friction interface model. The approach has been validated through the comparison with experimental tests on in-scale benchmarks: a circular arch, made of wood blocks bonded by mortar, subject to opening of the abutments; a cross vault, made of plastic blocks with dry joints, subject to opening, shear and tilting-plane tests.

The proposed approach has proven to be quite robust. The experimental results have been reproduced with a high degree of accuracy both in the case of planar and space structures, with both dry joints and mortar joints with low cohesion. The advantage of the friction interface model is that it requires the definition of a low number of parameters, which can be easily obtained by simple experimental tests, thus reducing modelling uncertainties.

This approach could, therefore, be applied to historical masonry structures, which are usually characterised by extremely low tensile strength and cohesion. The extension of the methodology to masonry characterised by high cohesion should be demonstrated. Furthermore, it is worth noting that this kind of modelling could be applied to masonry vaults characterised by regular apparatus, which is not always the case when historical structures are dealt with.

Future research includes the use of this method of analysis to simulate the behaviour of real masonry vaults. In this case the influence of other parameters not considered in this study, such as the presence of backfill or the influence of boundary walls, should be taken into account. Moreover, this modelling technique will allow to

investigate the influence of different block-patterns, or different building techniques, and the consequent different collapse mechanisms.

Acknowledgements

The authors are extremely grateful to A.M. D'Altri for fruitful discussion about numerical issues and for having shared his expertise in the definition of numerical parameters for implicit dynamic analysis with Abaqus.

References

Abaqus/CAE User's Manual, 2019.

Abdulla K.F., L.S. Cunningham and M. Gillie. 2017. Simulating masonry wall behaviour using a simplified micro-model approach, *Engineering Structures* 151: 349–365.

Alforno M., C. Calderini, A. Monaco and F. Venuti. 2019. Numerical modelling of masonry vaults with different brick pattern, *Proceedings of the IASS Annual Symposium 2019*, Barcelona.

Block P. and J. Ochsendorf. 2007. Thrust network analysis: a new methodology for three-dimensional equilibrium. *Journal of the International Association for Shell and Spatial Structures* 48(3):167–173

Bui T.T., A. Limam, V. Sarhosis and M. Hjiaj. 2017. Discrete element modelling of the in-plane and out-of-plane behaviour of dry-joint masonry wall constructions, *Engineering Structures* 136: 77–94.

Calderini C. and S. Lagomarsino. 2008. A micromechanical inelastic model for historical masonry, *Journal of Structural Engineering* 134: 209-220.

Carfagnini C., S. Baraccani, S. Silvestri and D. Theodossopoulos. 2018. The effects of in-plane shear displacements at the springings of Gothic cross vaults, *Construction and Building Materials* 186: 219–232.

Carr A.J., D.V. Jáuregui, B. Riveiro, P. Arias and J. Armesto. 2013. Structural evaluation of historic masonry arch bridges based on first hinge formation. *Construction and Building Materials*, 47:569-578.

Cascini L., R. Gagliardo and F. Portioli. 2020. LiABlock_3D: A Software Tool for Collapse Mechanism Analysis of Historic Masonry Structures. *International Journal of Architectural Heritage* 14(1): 75-94.

Creazza G., R. Matteazzi, A. Saetta and R. Vitaliani. 2002. Analyses of masonry vaults: a macro approach based on three-dimensional damage model, *Journal Structural Engineering* 129 (5): 646.

D'Altri A., S. de Miranda, G. Castellazzi and V. Sarhosis. 2018. A 3D detailed micro-model for the in-plane and out-of-plane numerical analysis of masonry panels, *Computers and Structures* 206:18–30.

D'Altri, A. M., F. Messali, J. Rots, G. Castellazzi and S. de Miranda. 2019a. A damaging block-based model for the analysis of the cyclic behaviour of full-scale masonry structures. *Engineering Fracture Mechanics* 209:423–48.

D'Altri A.M., S. De Miranda, G. Castellazzi, V. Sarhosis, J. Hudson and D. Theodossopoulos. 2019b. Historic barrel vaults undergoing differential settlements, *International Journal of Architectural Heritage*, 1-14

D'Altri A.M, V. Sarhosis, G. Milani, J. Rots, S. Cattari, S. Lagomarsino, E. Sacco, A. Tralli, G. Castellazzi and S. de Miranda. 2019c. Modeling Strategies for the Computational Analysis of Unreinforced Masonry Structures: Review and Classification. *Archives of Computational Methods in Engineering*. https://doi.org/10.1007/s11831-019-09351-x

Fabbrocino F., G. Ramaglia, G.P. Lignola and A. Prota. 2019. Ductility-based incremental analysis of curved masonry structures. *Engineering Failure Analysis* 97: 653-675.

Heyman J. 1966. The stone skeleton. *International Journal of Solids and Structures*, 2(2):249–279

Hibbitt, H. D., Karlsson, B. I. 1979. Analysis of Pipe Whip, *EPRI*, Report NP–1208.

Lourenço, P.B., J. G. Rots and J. Blaauwendraad. 1995. Two approaches for the analysis of masonry structures - micro and macro-modeling, *HERON* 40 (4): 313-340.

Lourenço, P.B. 1996. Computational Strategies for Masonry Structures, PhD-Thesis, *Delft University of Technology*, Delft, The Netherlands, ISBN 90-407-1221-2.

McInerney J. and M.J. DeJong. 2015. Discrete element modeling of groin vault displacement capacity, *International Journal of Architectural Heritage* 9(8): 1037–49.

Milani, G., M. Rossi, C. Calderini and S. Lagomarsino. 2016. Tilting plane tests on a small-scale masonry cross vault: Experimental results and numerical simulations through a heterogeneous approach, *Engineering Structures* 123: 300-312.

Milani, G. and A. Tralli. 2012. A simple meso-macro model based on SQP for the non linear analysis of masonry double curvature structures, *International journal of solids and structures* 49 (5):808-834.

Portioli F., L. Cascini, C. Casapulla and M. D'Aniello. 2013. Limit analysis of masonry walls by rigid block modelling with cracking units and cohesive joints using linear programming, *Engineering Structures* 57:232–47.

Portioli F. and L. Cascini. 2017. Large displacement analysis of dry-jointed masonry structures subjected to settlements using rigid block modelling, *Engineering Structures* 148:485–496.

Ochsendorf, J.A. 2002. Collapse of masonry structures. Dissertation, Department of Engineering, *Cambridge University*, Cambridge.

Ramaglia G., Lignola GP, Prota A. 2016. Collapse analysis of slender masonry barrel vaults, *Engineering Structures* 117: 86-100.

Rhinoceros User's Guide, v.5.4, 2018.

Riveiro B., M. Solla, I. De Arteaga, P. Arias and P. Morer. 2013. A novel approach to evaluate masonry arch stability on the basis of limit analysis theory and non-destructive geometric characterization. *Automatic in Construction* 31: 140-148.

Rossi M., C. Calderini, B. Di Napoli, L. Cascini and F. Portioli. 2020. Structural analysis of masonry vaulted staircases through rigid block limit analysis. *Structures* 23: 180-190.

Rossi, M., C. Calderini and S. Lagomarsino. 2016. Experimental testing of the seismic in-plane displacement capacity of masonry cross vaults through a scale model, *Bulletin of Earthquake Engineering* 14: 261-281.

Rossi M., C. Calvo Barentin, T. Van Mele and P. Block. 2017. Experimental study on the behaviour of masonry pavilion vaults on spreading supports, *Structures* 11:110-120.

Sarhosis V. and J. Lemos. 2018.A detailed micro-modelling approach for the structural analysis of masonry assemblages*, Computers and Structures* 206: 66-81.

Smoljanovic H., Zivaljic, Z. Nikolic and A. Munjiza. 2018. Numerical analysis of 3D dry-stone masonry structures by combined finite-discrete element method, *International Journal of Solids and Structures 136: 150-167.*

Theodossopoulos, D., B.P. Sinha, A.S. Usmani and A.J. Macdonald. 2002. Assessment of the structural response of masonry cross vaults, *Strain* 38: 119–127.

Theodossopoulos, D., B.P. Sinha and A.S. Usmani. 2003. Case Study of the Failure of a Cross Vault: Church of Holyrood Abbey, *Journal of Architectural Engineering* 109-117

Torres B., El. Bertolesi, P.A. Calderón, J.J. Moragues and J.M. Adam. 2019. A full-scale timbrel cross vault subjected to vertical cyclical displacements in one of its supports, *Engineering Structures* 183:791–804.

Van Mele T., J. McIrney, M.J. DeJong and P. Block. 2012. Physical and computational discrete modelling of masonry vault collapse, *Proceedings of Structural analysis of historical constructions SAHC 2012*, Wrocklaw, Poland.

Zhao C., Y. Xiong, X. Zhong, Z. Shi and S. Yang. 2020. A two-phase modeling strategy for analyzing the failure process of masonry arches, *Engineering Structures* 212: 110525